Wave-formed sediment ripples: Transient analysis of ripple spectral development

Joseph P. Davis and David J. Walker
School of Civil and Environmental Engineering, University of Adelaide, Adelaide, South Australia, Australia

Murray Townsend
Department for Environment and Heritage, Adelaide, South Australia, Australia

Ian R. Young
Swinburne University of Technology, Hawthorn, Melbourne, Australia

Received 2 February 2004; revised 8 April 2004; accepted 26 May 2004; published 27 July 2004.

[1] A new method has been developed that models the changes a wave-formed rippled sediment bed undergoes as it is actively evolving between two given equilibrium states due to a change in surface wave conditions. The transient analysis of rippled beds has received very little attention within the literature. Dynamic changes within ripple parameters have implications for the estimation of flow dissipation and sediment transport by changing the bottom roughness height. The method uses the spectral density function of the rippled bed and is based on a series of ripple growth and ripple transition experimental tests. The ripple evolution model was developed from the well-known Logistic Growth Law. Fitting the general solution of the logistic nonlinear differential equation to the experimental data enabled the evolution rate of the bed to be determined for each experimental test. It was concluded that there was no difference between the evolution rate determined from the ripple growth tests and the ripple transition tests. This indicated that the two types of growth are special cases of the same evolution processes, which is adequately modeled by the logistic growth equation. A functional dependence was established between the ripple evolution rate and the Shields parameter. This allows the evolution rate to be estimated from flow and sediment properties. The estimation of the rate at which rippled sediment beds evolve under a variable sea state has the potential to lead to significant improvements to the way ripple transition and hence bottom roughness is approximated in coastal wave models. *INDEX TERMS:* 3045 Marine Geology and Geophysics: Seafloor morphology and bottom photography; 4219 Oceanography: General: Continental shelf processes; 4546 Oceanography: Physical: Nearshore processes; *KEYWORDS:* spectral analysis, nearshore processes, sediment ripples

Citation: Davis, J. P., D. J. Walker, M. Townsend, and I. R. Young (2004), Wave-formed sediment ripples: Transient analysis of ripple spectral development, *J. Geophys. Res.*, *109*, C07020, doi:10.1029/2004JC002307.

1. Introduction

[2] Seabed morphology in shallow coastal seas is composed of a large number of sediment structural types of differing sizes and shapes. These structures range from large bars and dunes, which control the overall hydrodynamics of a coastal sea, to the smaller-scale bedforms such as ripples and animal mounds, which will modify the wave and current boundary layer structure [*Nielsen*, 1992]. The most dynamic of these types are the small-scale bedforms, which can change in the order of hours depending on the hydrodynamic flow conditions and biological activity of the bed [*Amos et al.*, 1988; *Drake and Cacchione*, 1989; *Wheatcroft*, 1994]. The small-scale bedforms are extremely important as they act to change the pressure distribution, through flow separation and wake formation, within the bottom boundary layer, which in turn enhances the physical processes that act on or across the sediment-water interface [*Dade et al.*, 2001; *Huettel and Webster*, 2001; *Jorgensen and Boudreau*, 2001]. Of major interest to coastal researchers is the effect ripples have on the hydraulic roughness of the seabed and sediment entrainment rates. Hence there has been a high level of interest within the literature regarding the prediction and growth of rippled sediment beds, especially under the action of waves [e.g., *Nielsen*, 1981, 1992; *Mogridge et al.*, 1994; *Wiberg and Harris*, 1994; *Marsh et al.*, 1999; *O'Donoghue and Clubb*, 2001; *Faraci and Foti*, 2002]. An area in which there has been very little research is determining the rate at which rippled beds change when they are actively changing to reach equilibrium with the surface wave field.

0148-0227/04/2004JC002307$09.00

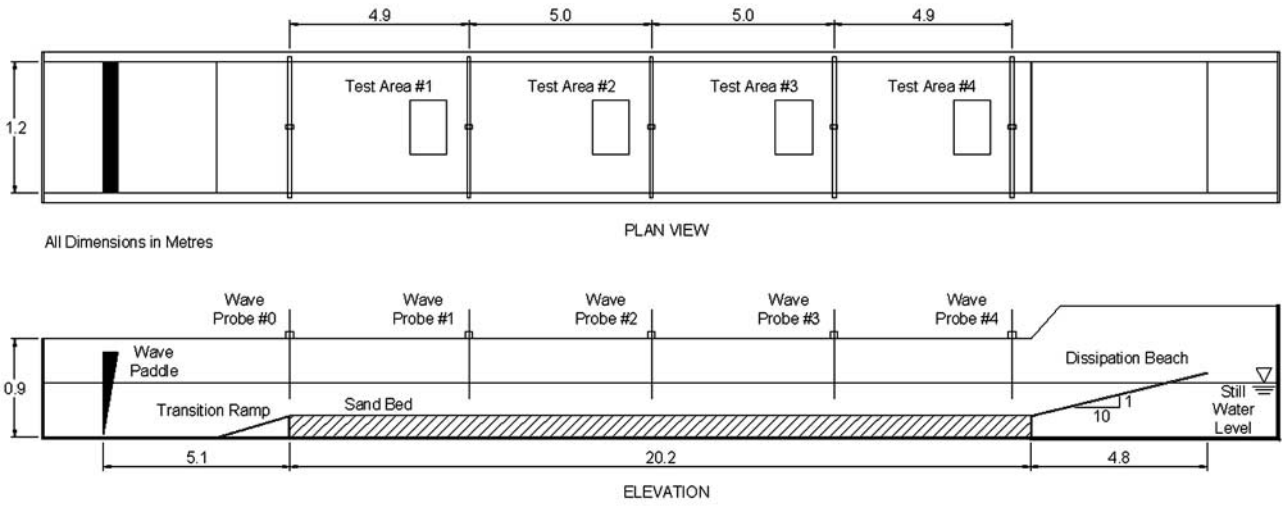

Figure 1. Plan and elevation views of the wave flume.

[3] A number of authors have developed movable bed roughness models to account for the highly dynamic nature of wave-formed rippled beds and incorporated these into flow and sediment transport models [*Grant and Madsen*, 1982; *Graber and Madsen*, 1988; *Tolman*, 1994, 1995]. However, these movable bed roughness models do not contain ripple evolution submodels, but assume that ripple growth rates are much higher than the rate at which the flow conditions change. This effectively means that the rippled bed is in constant equilibrium with the flow conditions. On the basis of field observation of ripple dynamics by *Amos et al.* [1988]; [*Wheatcroft*, 1994]; *Bell and Thorne* [1997]; *Traykovski et al.* [1999]; *Doucette* [2002], and *Moore and Jaffe* [2002], this will generally not be the case.

[4] There has been substantial work undertaken on developing growth models for current-formed ripples growing from flat bed conditions [e.g., *Coleman and Melville*, 1996; *Nikora and Hicks*, 1997; *Baas*, 1999]. The main focus of these studies was to determine the rate at which the ripples change within fluvial environments. Conversely, there has been little work undertaken on determining the rate at which wave-formed rippled beds will evolve due to a change in the surface wave spectra. A limited set of previous laboratory studies have observed and recorded wave-formed ripples growing from flat bed conditions. *Marsh et al.* [1999], based on a series of wave flume experiments, suggested that wave-formed ripples would attain equilibrium with the flow conditions after 30 to 40 min. This time was determined by visually observing the bed. The authors presented a number of ripple profiles with time, but this was done to confirm that the bed had reached equilibrium, not to model ripple growth. *O'Donoghue and Clubb* [2001] undertook a series of experiments using an oscillating water tunnel that investigated ripple formation under both high- and low-mobility conditions. They found that under high-mobility conditions, wave-formed ripples became stable after approximately 30 min, while under low-mobility conditions the ripples could take many hours to attain equilibrium with the flow conditions. As with *Marsh et al.* [1999], they based their estimate of the equilibrium time on visual observations of the developing ripple bed. *Faraci and Foti* [2002] undertook a series of flume-based tests using irregular waves. From their tests, they indicated that wave-formed ripples would take in the order of 15 min to reach equilibrium. However, their estimate may have been slightly low due to their focus on individual ripples, not the rippled bed as a whole (a point to be expanded upon in subsequent sections). However, *Faraci and Foti* [2002] did measure and plot ripple parameters developing over time as the ripples grew from flat bed conditions, but did not attempt to develop a growth model from their data set. To the authors' knowledge, there have been no studies that have attempted to developed a ripple evolution model to describe the transient nature of wave-formed rippled beds.

[5] The current paper investigates the rate at which wave-formed rippled beds attain equilibrium within a flume setting; however, a different approach is taken in that the rippled bed is considered to develop as a whole through the use of the rippled bed's spectral density function. Two equilibrium states were considered, the first being a flat bed condition that is in equilibrium with a no-wave surface condition, and the other being a fully developed ripple bed that is in equilibrium with the surface waves that originally formed the bed. Using a spectral analysis method, changes in the ripple height, length, and/or shape can be considered as an energy transfer process. The flow conditions within the near-bottom regime imparts kinetic energy to the individual ripple grains, which are moved and built up into ripple forms. This building-up process results in the ripple grains increasing their level of potential energy relative to a flat bed condition.

2. Experimental Procedure and Setup

[6] A series of experiments observing the growth and transition of rippled bed morphology due to a change in the irregular surface wave conditions was undertaken within the wave flume located in the Robin Hydraulic Laboratory at the University of Adelaide, Australia. The wave flume used

has a total length of 30 m and a width of 1.2 m, with an overall depth of 900 mm (refer to Figure 1).

[7] The experiments were undertaken using two types of sand. The first sand (type 1) was finer and had a mean grain diameter (D_{50}) of 242 μm, while the second sand (type 2) was slightly coarser with a D_{50} of 372 μm. Both sand types were quartz based and had coefficients of uniformity (C_u) of approximately 1.5. Three irregular surface wave peak frequency conditions were used: 0.8, 1.0, and, 1.2 Hz. Tests were undertaken with variable water depths within the flume to increase the interaction between the surface waves and the bottom sediment bed. Wave conditions were monitored along the flume using a set of five surface-penetrating resistance wave probes. Each wave probe was located on the centerline of the flume. For the experiments contained within this study, only one sediment test area was utilized, which was located directly in front of wave probe 1 (refer to Figure 1). Test area 1 was at a distance of 9 m from the wave paddle. The sediment surface was scanned underwater using an Automated Sediment Interface Laser Scanner referred to as the ASILS system. The ASILS was designed and developed in-house and consists of a laser displacement sensor suspended approximately 95 mm above the sand bed from a computer controlled X-Y positional table. The laser sensor used was a type "LAS-8010V" visible laser analog sensor produced by Nippon Automation Company Ltd. *O'Donoghue and Clubb* [2001] also used this type of laser sensor to measure rippled beds. The vertical resolution of the ASILS system was on the order of 0.2 mm. An important requirement of the system was the ability to scan the sediment surface underwater while waves were being run along the flume. To achieve this goal the laser sensor was encased in a clear 80-mm-diameter Perspex tube, which passed through the air-water interface [*Davis et al.*, 2003]. The measuring head of the ASILS was parked in a down wave position between each of the 5-min scans to minimize the disruption to the flow patterns near the bed.

[8] As outlined in the introduction, two types of experimental tests were undertaken, beginning with tests observing the growth of ripple beds and tests observing the transition of rippled beds. These two tests will be described in greater detail in the subsequent sections. During both types of tests, the waves were run continuously with the same spectral attributes. The irregular wave generation software used a continuous random signal generator which conformed to a predefined distribution. This signal was repeated over a time period depending on the frequency of waves generated. For the three surface wave frequency conditions used, this repeating period was 10.67 min for the 0.8 Hz waves, 8.53 min for the 1.0 Hz waves, and 7.12 min for the 1.2 Hz waves. This meant that the surface wave spectrum was repeated at least 14 times during the shortest test analyzed during this study.

[9] Each long sectional scan was 1000-mm long with a primary spacing of 1.56 mm, which gave a total of 640 data points taken from the sediment surface as a one-dimensional (1-D) scan. The raw data array was filtered using a fast Fourier transform (FFT) band-passing filter to remove the longer wavelengths (red noise) present in the data set before calculating the spectral density function.

[10] The spectral density function for the transient tests was formed by breaking each of the 1-D data vectors (each containing 640 data points) into five equal sections, each with 128 data points. The spectral density function of each of these sections was calculated with a band width of 128, giving a spectral density function with 2 degrees of freedom. The spectral estimate of each 1-D section was then averaged to give a spectral estimate of the sediment surface with 10 degrees of freedom. The spectral density function was calculated using the power-spectral-density (PSD) function within MATLAB's Signal Processing Toolbox, which utilizes Welch's averaged, modified periodogram method (Mathworks, Signal Processing Toolbox, available at www.mathworks.com, 2002). The power spectrum (mm^2) estimated via the PSD routine was multiplied by twice the sample interval (mm) to give an estimate of the 1-D variance spectrum (mm^3) for the sediment surface.

3. Ripple Parameters and the Ripple Spectrum

[11] In addition to the spectral description, two ripple parameters were defined from the 1-D ripple spectrum to provide a measure of the characteristic ripple height and length of the sediment bed. The characteristic ripple height is a direct analogy to the significant wave height used within water wave theory and is defined from the bottom ripple spectrum as

$$\eta_c = 2.8\sqrt{\int_{f_{s1}}^{f_{s2}} S_r(f_s)\,df_s}, \tag{1}$$

where η_c is the characteristic ripple height (millimeters), S_r is the ripple variance spectrum (mm^3), f_s is the spatial frequency (mm^{-1}) and f_{s1}, and f_{s2} are the upper and lower bounds defining the ripple spatial frequencies present in the spectrum. The multiplication factor of 2.8 used in equation (1) was determined by fitting a straight line between the characteristic ripple height and the variance of the ripple series for a number of equilibrium rippled beds. The characteristic ripple height was determined for the rippled bed using the zero upcrossing method as outlined by *Goda* [2000]. The characteristic ripple length is defined as

$$\lambda_c = \frac{\int_{f_{s1}}^{f_{s2}} S_r^4(f_s)\,df_s}{\int_{f_{s1}}^{f_{s2}} f_s S_r^4(f_s)\,df_s}, \tag{2}$$

where λ_c is the characteristic ripple length (millimeters). *Young* [1995] discussed the weighted integral used in equation (2) in relation to the determination of the peak frequency of surface wave spectrum and found that it was the most reliable technique available.

[12] The ripple spectrum was nondimensionalized using the flow and sediment properties. This was undertaken so that equilibrium spectra formed under different waves with different sediment types could be compared mathematically. Two nondimensional numbers were developed that use the two length scales applicable to oscillatory motion over movable sediment beds, the peak orbital excursion diameter (d_{op}), and the 50 percentile grain size diameter (D_{50}). The

Table 1. Summary of the Ripple Growth Tests Undertaken

Growth Test ID	Water Depth, m	Sand D_{50}, μm	Wave Parameters[a]		Flow Parameters		Dimensionless Variables[b]			
			σ_p, Hz	H_s, m	U_p, m/s	d_{op}, m	Re_d	Re	θ	ψ
G01	0.286	242	0.80	0.079	0.153	0.061	41.7	5882	0.105	7.6
G02	0.184	242	0.80	0.067	0.183	0.072	49.7	8368	0.137	10.8
G03	0.187	242	0.80	0.070	0.189	0.075	51.3	8906	0.144	11.5
G04	0.205	372	0.80	0.083	0.214	0.085	87.5	11035	0.133	9.2
G05	0.208	372	0.80	0.082	0.209	0.083	85.8	10618	0.129	8.8
G06	0.287	242	0.84	0.082	0.154	0.058	41.9	5676	0.107	7.6
G07	0.287	242	0.84	0.082	0.154	0.058	42.0	5713	0.108	7.7
G08	0.282	242	0.99	0.095	0.168	0.054	42.3	4927	0.118	7.8
G09	0.288	242	0.99	0.092	0.157	0.050	40.0	4373	0.108	7.0
G10	0.205	372	0.99	0.093	0.223	0.072	86.8	8778	0.146	9.0
G11	0.184	372	0.99	0.080	0.208	0.067	81.9	7823	0.133	8.0
G12	0.284	242	0.99	0.089	0.156	0.050	39.2	4200	0.105	6.7
G13	0.289	242	1.00	0.091	0.157	0.050	39.4	4249	0.106	6.8
G14	0.288	242	1.00	0.091	0.157	0.050	39.2	4193	0.105	6.7
G15	0.288	242	1.04	0.089	0.147	0.045	36.8	3550	0.097	5.9
G16	0.186	242	1.18	0.065	0.149	0.040	37.2	3169	0.106	6.0
G17	0.183	242	1.18	0.065	0.152	0.041	37.9	3298	0.109	6.3
G18	0.154	372	1.14	0.075	0.208	0.058	80.5	6523	0.140	7.8
G19	0.184	372	1.14	0.080	0.190	0.053	73.2	5404	0.122	6.4
G20	0.288	242	1.22	0.076	0.098	0.026	23.5	1231	0.055	2.4

[a]Calculated from the measured surface wave spectrum.
[b]Calculated from standard linear wave theory using H_s, σ_p, and the water depth.

peak orbital excursion diameter was calculated from the surface wave spectrum. The first nondimensional number transforms the rippled bed's spectral energy as

$$S' = \frac{S_r}{d_{op}^2 D_{50}}, \tag{3}$$

while the second transforms the spatial frequencies of the rippled bed as

$$f_s' = f_s^2 d_{op} D_{50}. \tag{4}$$

The nondimensional form of the ripple spectra resulted in spectra formed under different flow conditions and on different sediment beds showing similar nondimensional peak spectral energy levels, nondimensional peak spatial frequencies, and shapes. This enabled the ripple spectrum from different tests to be compared and modeled. It has to be emphasized that the nondimensional spectrum described by equations (3) and (4) does not represent a variance spectrum, and hence the area under the spectral curve will not equal the variance of the series.

4. Rippled Bed Growth

[13] To develop a ripple evolution model, the growth of ripples from a no-ripple (flat bed) condition needs to be understood and parameterized. A no-ripple state occurs in nature when there has been an absence of suitable wave conditions to form ripples. Field studies by *Amos et al.* [1988] indicate that benthic organisms will degrade rippled beds to a "flat" bed condition within 4 to 6 hours. However, in general, numerical models start from a no-flow condition and are then ramped up as the simulation proceeds. Similarly, parameterizations of rippled beds would also require ramping up from a flat bed condition as the simulation starts. Hence the growth characteristics of rippled beds growing from flat bed conditions are required in the ripple evolution model. This section describes a series of experiments that monitored the growth of rippled beds under the action of an irregular surface wave field as they grew from a no-rippled state. The analysis focuses on the development of the ripple spectrum and spectral energy with time under a variety of flow and sediment conditions. Please note that a sediment bed that has no ripples will be referred to within this publication as a no-ripple condition. This is in preference to calling the bed "flat," as sediment beds are never flat, but will always have some level of background roughness.

[14] Table 1 lists the experimental tests undertaken within this section. The first column in Table 1 lists the experiment identification code. The peak bottom orbital velocity (U_p) and peak orbital excursion diameter (d_{op}), shown in Table 1, were calculated from the root mean squared (rms) velocity (U_{rms}) determined from the surface wave spectrum using a method outlined by *Soulsby* [1987]. The peak bottom orbital velocity was calculated as $U_p = 1.42\sqrt{2}U_{rms}$ [see *Traykovski et al.*, 1999], while the peak orbital excursion diameter was calculated as $d_{op} = U_p/(\pi\sigma_p)$, where σ_p is the peak surface wave frequency. The dimensionless variables listed in Table 1 were calculated from standard linear theory and are included to provide a scale of the flow parameters compared to sediment parameters. The sediment Reynolds number (Re_d) was calculated using the D_{50} of the sediment as a length scale, while the flow Reynolds number (Re) used the orbital excursion amplitude calculated from linear theory ($A = do/2$) as a length scale. The Shields parameter (θ) was calculated using the skin friction roughness and as such does not take into account ripple forms that were changing during the tests. The grain roughness friction factor was calculated using the relationship of *Swart* [1974] with a roughness height of $2.5D_{50}$. The mobility number (ψ) was calculated using the D_{50} of the sediment.

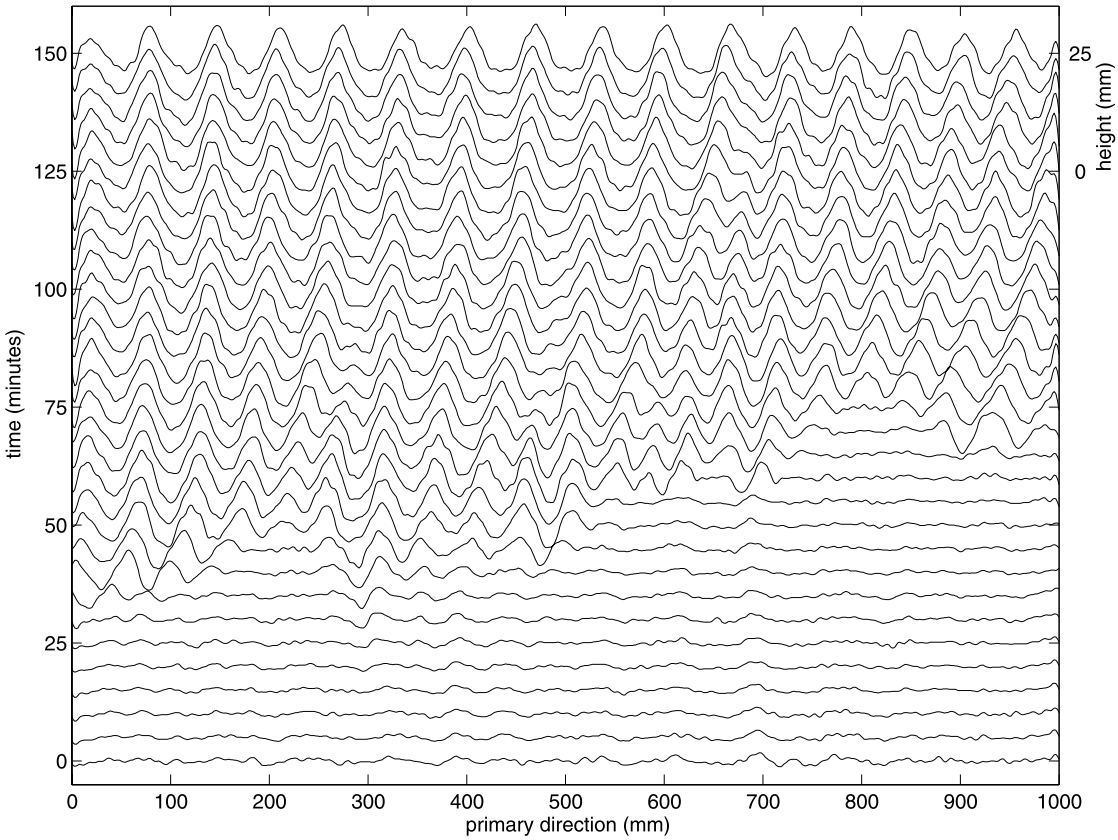

Figure 2. Example plot showing typical ripple growth with time (Δt = 5 min). Surface waves are moving from left to right across the bed. Left-hand axis indicates the test time while the upper right-hand axis provides a scale of ripple height.

[15] The growth tests shown in Table 1 were started with the sediment bed in a no-ripple condition. Ripples were formed on the sediment surface by running irregular waves conforming to a standard JONSWAP (γ = 3.3) spectrum along the flume for a period of 2.5 hours. After this time the waves and sediment ripples were considered to be at equilibrium. As the rippled bed was developing, a 1-m-long section of the rippled bed along the centerline of the flume was scanned every 5 min. This provided 31 long sections in total, which showed the growth of the rippled bed from a no-ripple condition over time. Figure 2 shows an example of the data that were obtained from the ripple growth tests. This bed is shown as test G05 in Table 1 and was formed using type 2 sediment (D_{50} = 372 μm) under a JONSWAP wave spectrum with a peak frequency of 0.8 Hz and a significant wave height of 82 mm.

[16] As can be seen in Figure 2, the rippled bed takes a period of time to initiate ripple formation, but once ripples start to appear on the surface the bed develops quickly. Once the ripples have developed, they no longer change and can be considered to have equilibrated with the flow conditions. Ripples along the bed typically do not form at the same time, but one or two individual ripples will form at a given location in isolation, then other ripples will form spreading out in both the up-wave and down-wave directions. *Faraci and Foti* [2002] also noted this form of growth in their irregular wave tests. The growth mechanism follows the original suggestion of *Bagnold* [1946] that ripples need to pass through the rolling grain preliminary state. Once the sediment at a given location has built up enough via the rolling grain mechanism, it starts to disrupt the bottom boundary layer, and flow separation occurs with a vortex being shed in the wake of the ripple. The larger velocity associated with the vortex causes sediment to be scoured behind the ripple, and hence the ripple grows rapidly. As the flow is oscillating, these vortices and the associated turbulence are carried both in the up-wave and down-wave directions. Thus the ripples spread out in both directions from the original perturbation of the sediment surface.

[17] There are a number of ways in which the ripple height and length can be estimated during the preliminary growth stages of the rippled bed. Individual ripples can be chosen and then followed through the time series, measuring the height and length of the particular ripple at each time step. *Faraci and Foti* [2002], who used photographs to determine individual ripple heights and lengths at each time step, undertook this method. For the data shown in Figure 2 the first ripple appears at 30 min, while the total bed does not become fully rippled until 75 min. Hence focusing on a particular ripple form may give an unrealistic picture of the time rippled beds take to develop. A more concise way to describe the growth of rippled beds is to observe the way the ripple spectrum develops with time. This assumes that the rippled bed can be considered as a moving random field of bottom elevations. The developing rippled bed can then

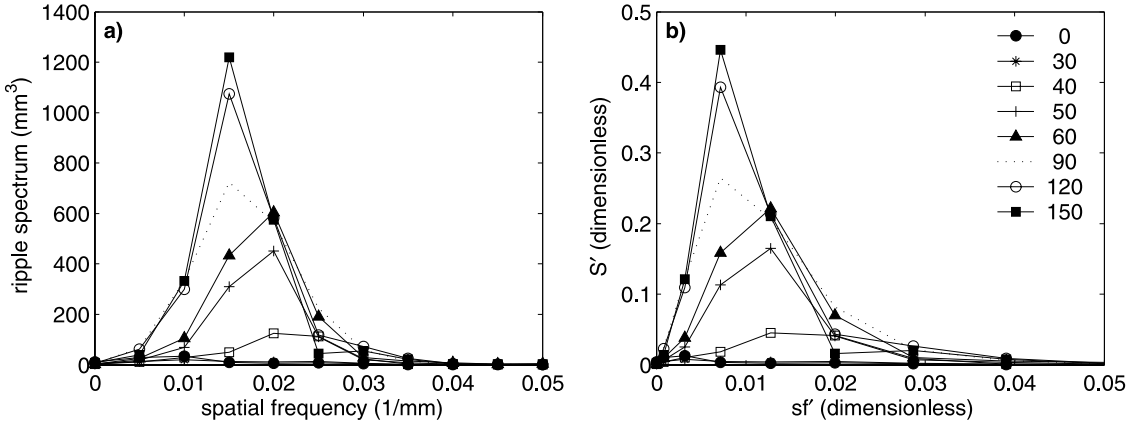

Figure 3. Example plot showing typical ripple spectrum growth with time. (a) Dimensional spectrum calculated from the sediment surface. (b) Ripple spectrum nondimensionalized by the flow and sediment conditions.

be characterized as a whole without bias being given to any particular area of the bed. Figure 3 shows the development of both the dimensional spectra and the nondimensional spectra with time. The nondimensional scaling was undertaken via equations (3) and (4). The data used to produce Figure 3 are the same as those shown in Figure 2.

[18] Figure 3 shows that the growth of the ripple spectrum starts at the higher spatial frequencies and shifts to the lower frequencies as the ripples start to develop. This indicates that the ripples are lengthening as their height is increasing. *Jain and Kennedy* [1974] suggested a mechanism for the evolution of the current-formed ripple spectra. They suggest that the speed of sediment ripples along the bed is dependent on the length of the ripples; hence ripples will be dispersive (longer ripples will move faster along the bed than shorter ripples). Since individual ripples are not able to move through each other, over time all ripples will become larger and more uniform. *Jain and Kennedy* [1974] called this process "the variance cascade" as ripples cascade into each other. There is some evidence of this process in the spatial data shown in Figure 2. A number of the original smaller ripples are swallowed during the evolution process by adjacent larger ripples. However, this effect is small in the current tests due to the ripples only moving small distances during the 2.5-hour test period.

[19] As with the spatial ripple data (refer to Figure 2) the spectral energy takes approximately 30 min to increase above a background level. Once the ripples have started to grow their spectral energy increases consistently until the ripples have equilibrated with the flow conditions. Observing the spectra will give a good indication of whether the bed has reached equilibrium during a given test. In Figure 3 the spectral energy is stable after 120 min of run time.

[20] From the ripple spectrum a characteristic ripple height and length can be calculated using equations (1) and (2). This allows a time series to be plotted showing the growth of ripple parameters through time (refer to Figure 4). A measure of the ripple steepness can be calculated by simply taking the ratio of the ripple height to ripple length. These estimates of ripple height and length are based on the bed as a whole and do not map the growth of individual ripples. As with Figures 2 and 3, the data used to form Figure 4 came from test G05.

[21] Figure 4 provides another way the ripple bed can be viewed changing with time. The ripple length is interesting in Figure 4, as it starts off at a very high level, then falls to a minimum, and then rises again to an equilibrium level. The background spectral energy of the bed, although very small in energy, has a peak spatial frequency (length) that is much smaller than the spatial frequencies associated with ripple forms. As the ripples grow, this background level of roughness is washed out and replaced with small ripples, which in turn lengthen into equilibrium ripples. Hence the peak spatial frequency drops to a minimum from some background level, then grows again. The ripple steepness is calculated here as the ratio of ripple height over the ripple length. The unrealistic longer lengths calculated during the start of the test do not affect the steepness, as the ripple height is small during this period.

5. Rippled Bed Transition

[22] As outlined above, a number of authors have investigated the growth of rippled beds under the action of waves from a no-ripple condition. However, no study has been found by the authors that has parameterized the transition of rippled beds from one equilibrium state to another. The transition of ripples due to a change in wave direction or energy has been widely observed within the field [*Amos et al.*, 1988; *Wheatcroft*, 1994; *Drake and Cacchione*, 1989; *Bell and Thorne*, 1997; *Traykovski et al.*, 1999; *Doucette*, 2002; *Moore and Jaffe*, 2002]. How an established ripple bed will change under flow conditions that are no longer in equilibrium with the bed is important in understanding the mechanism of ripple evolution. The time a rippled bed will take to reach equilibrium with the new flow conditions is likely to be a function of the energy within the flow and the energy that is required to move the individual sand grains [*Wiberg and Smith*, 1985]. Understanding both the mechanism of change and the time a rippled bed will take to reach a new equilibrium is required to develop a ripple evolution model. This section presents a series of experimental results used to investigate the changes rippled beds undergo when in the process of actively changing from one equilibrium state to another.

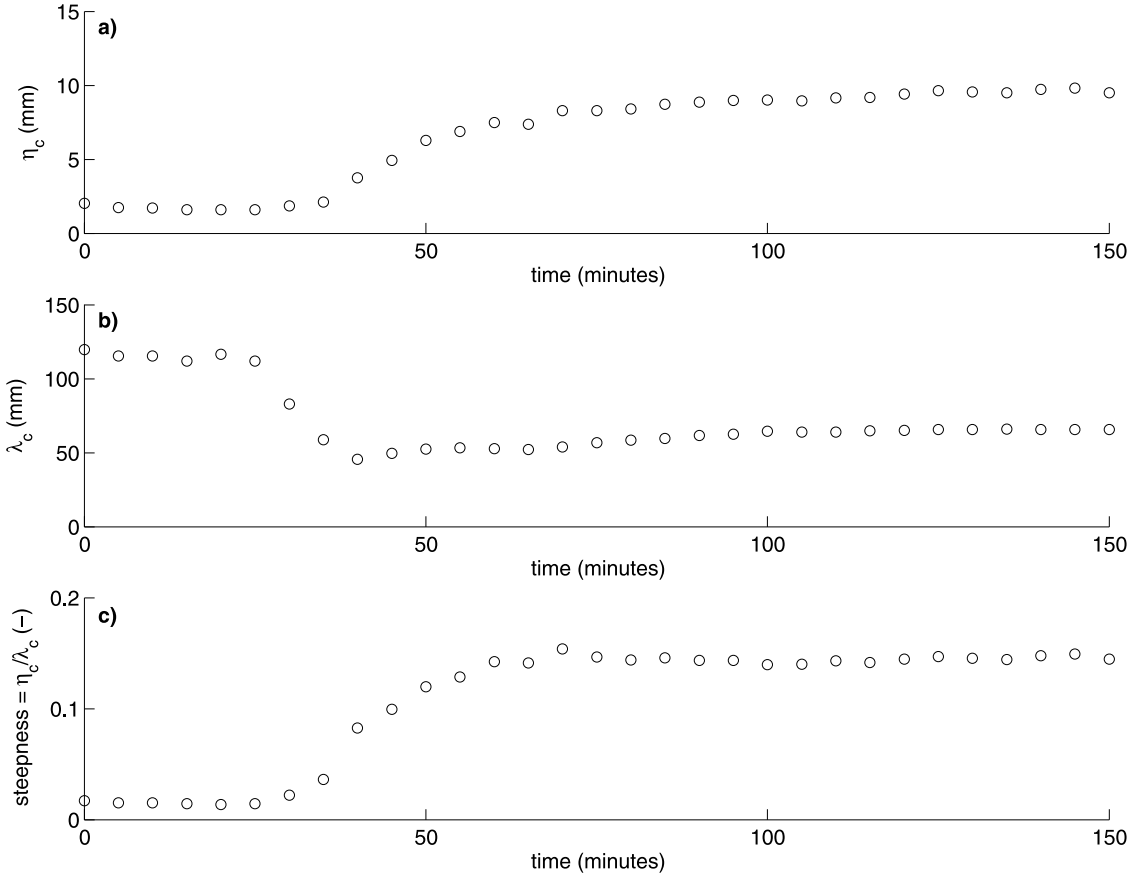

Figure 4. Growth of the example rippled bed parameters with time. (a) Ripple height. (b) Ripple length. (c) Ripple steepness.

[23] The transition tests were started with remnant equilibrium ripples already present on the surface from a previous experiment, which had been generated using different surface wave conditions. The waves conditions were changed and irregular waves were run over this bed for a period of 2 hours until the ripples had once more equilibrated with the surface wave conditions. As with the growth tests, a one-dimensional (1-D) sediment scan was taken every 5 min along the centerline of the flume. Transition tests provided 25 long sections of the rippled surface as the rippled bed transited to a new equilibrium configuration.

[24] Table 2 lists the experimental tests undertaken to observe ripple transition. The first column in Table 2 lists the experiment identification code. The second column gives the test ID of the experimental test that formed the original rippled bed. Please note the test ID shown starting with a "G" (Growth) are listed in Table 1, while those starting with a "T" (Transition) are listed in Table 2. All other parameters shown in Table 2 were calculated in the same way as outlined for Table 1.

[25] Figure 5 presents two examples of rippled beds actively changing under a changed surface wave spectrum. Figure 5a shows a rippled bed transitioning from a higher energy state back to a lower energy state. The high energy state represents a bed formed under experimental conditions listed in Table 1 as G05, while the low energy state is listed as T03 in Table 2. Figure 5b shows the opposite, with the

Table 2. Summary of the Ripple Transition Tests Undertaken

Transition	Original	Water	Sand	Wave Parameters[a]		Flow Parameters		Dimensionless Variables[b]			
Test ID	Test ID	Depth, m	D_{50}, μm	σ_p, Hz	H_s, m	U_p, m/s	d_{op}, m	Re_d	Re	θ	ψ
T01	G01	0.187	242	1.18	0.065	0.148	0.040	37.0	3152	0.105	6.0
T02	G07	0.287	242	1.22	0.075	0.098	0.026	23.5	1231	0.055	2.4
T03	G05	0.193	372	1.15	0.080	0.182	0.051	69.7	4882	0.114	5.8
T04	T08	0.184	372	1.15	0.081	0.192	0.053	73.6	5438	0.123	6.5
T05	T01	0.287	242	0.81	0.078	0.152	0.060	41.3	5753	0.103	7.4
T06	G17	0.284	242	0.81	0.079	0.154	0.061	42.1	5967	0.106	7.7
T07	T03	0.204	372	0.80	0.080	0.208	0.083	85.3	10506	0.128	8.7
T08	G19	0.208	372	0.80	0.081	0.207	0.083	85.2	10482	0.128	8.7
T09	G20	0.288	242	0.84	0.083	0.157	0.059	42.6	5886	0.110	7.9

[a]Calculated from the measured surface wave spectrum.
[b]Calculated from standard linear wave theory using H_s, σ_p, and the water depth.

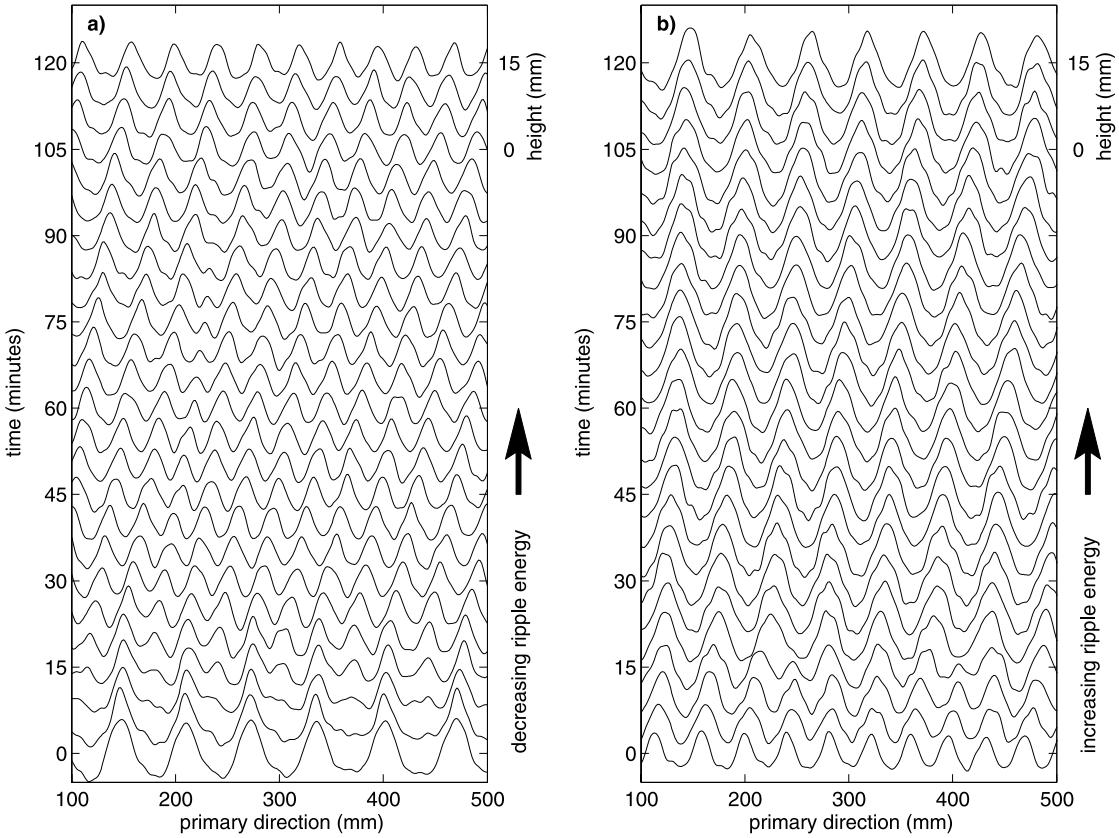

Figure 5. Example plot showing typical ripple transition under the action of surface waves that are out of equilibrium with the rippled bed (Δt = 5 min). (a) Change in the rippled bed as the ripple energy is decreasing. (b) Change in the rippled bed as the ripple energy is increasing.

bed transitioning from a lower energy state up to a higher state. The low energy state was formed by test T03 in Table 2, while the low energy state is listed as T07 in Table 2. The two examples were chosen because they were both generated using the same sediment diameter with similar wave heights.

[26] The first thing that can be noticed in Figure 5 is the change in ripple length between the equilibrium states. In Figure 5a the number of ripples in the 400-mm section grows from 6 to 10 in the 2-hour period, while in Figure 5b the number ripples reduces from 10 to 7 during the transition. This change in ripple length is brought about by a change in the surface wave frequency used in each of the experimental tests: a change from 0.8 to 1.2 Hz in Figure 5a and a change from 1.2 to 0.8 Hz in Figure 5b. This change in the surface wave frequency will correspond to a change in the length of the peak orbital excursion diameter. Small-scale wave-formed ripples such as these will generally scale to the orbital excursion diameter [*Nielsen*, 1981].

[27] The process by which this occurs is slightly different in each case. There is only finite space on the bed, and the bed adjusts to this space by either creating new ripples or swallowing older ripples. In Figure 5a the mechanism of length reduction is one in which new ripples form between the remnant ripples. The remnant ripples first become very steep and flat bottomed with their sides being eroded. New ripples start to form in the inter-ripple spacings. This is shown at a test time of 30 min with an exact doubling of the number of ripples present on the surface (from 6 to 12 at time of 30 min). During this time, there is an associated reduction in the ripple height as the sediment is redistributed between ripples. After this doubling the ripples then adjust to the flow conditions by growing slightly. This is achieved on the bed by a number of the newer ripples being swallowed by their neighboring ripples. In Figure 5b, however, the ripples will start to lengthen as they attempt to equilibrate with the new orbital excursion diameter. This lengthening process causes a number of ripples to be once again swallowed by their neighboring ripples. As the ripples are swallowed the surviving ripples grow in height as the sediment is once more redistributed across the bed. Figure 3 of *Marsh et al.* [1999] also shows this process where a ripple is swallowed by an adjacent ripple as the bed is adjusting to the flow conditions.

[28] Another observation gained from Figure 5 is the speed at which the ripples move. Figure 5 shows that the ripples moved between 25 and 100 mm in the 2-hour period. As the ripples' length changes, there is also a slight change in their speed, shown by the slope of the ripple crest line between each plot; hence the suggestion by [*Jain and Kennedy*, 1974] that ripples are dispersive is supported.

[29] As with the ripple growth data the ripple transition data can be viewed as a change in the spectral energy of the bed with time. Figures 6a and 6b show the ripple energy decreasing and were calculated from the data set shown by

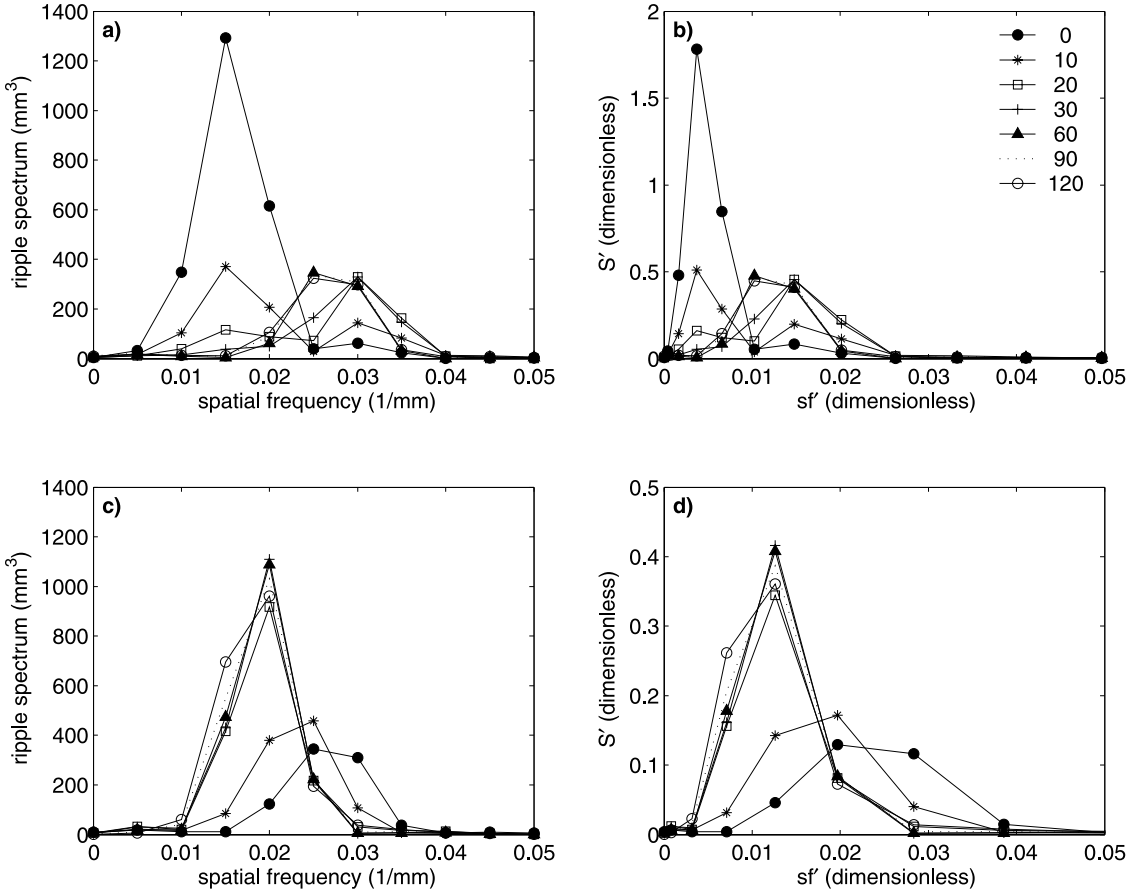

Figure 6. Example plots showing the ripple spectrum transition under the action of surface waves that are out of equilibrium with the rippled bed. (a) Dimensional and (b) nondimensional spectrum decreasing due to a lower wave energy state. (c) Dimensional and (d) nondimensional spectrum increasing due to a higher wave energy state.

Figure 5a, while Figures 6c and 6d show the increase in the ripple energy and were calculated from the data shown in Figure 5b. As with Figure 3, the left-hand side shows the dimensional spectra calculated from the bed, while the right subplots show the nondimensional spectra scaled by equations (3) and (4).

[30] The same trends that were evident in Figure 5 can also be seen in Figure 6. Figures 6a and 6b show the reduction of ripple energy due to a change in the surface wave spectra. The peak spectral energy has dropped with a corresponding increase in the peak spatial frequency of the bed. This relates to the ripples getting smaller and shorter. The peak spatial frequency increases quickly, and by 30 min it has doubled from a value of 0.015 to a value of 0.03. This was also evident in Figure 5a with a doubling in the number of ripple forms present on the surface by a time of 30 min. The bed then further adjusts to the flow conditions, with the ripples slightly increasing their length. This is shown in Figures 6a and 6b as a slight decrease in the peak spatial frequency to a final value of approximately 0.025. Figures 6a and 6b also show that the total area under the spectral curve has decreased, which represents an overall decrease in the potential energy of the bed. Figures 6c and 6d show an increase in the spectral energy of the bed due to a change in the surface wave field. As can be seen, the bed has increased its peak spectral energy, and there has been a decrease in the peak spatial frequency. This corresponds to an increase in ripple height and an increase in ripple length. The area under the spectral curve has also increased, which suggests an overall increase in the potential energy of the bed. The transition to a higher energy state shown in Figures 6c and 6d is much smoother than the transition, shown in Figures 6a and 6b, with the ripples decreasing continuously until they achieve their equilibrium peak spatial frequency. However, the time for both example beds to achieve near-equilibrium conditions was very similar. In both cases this was achieved after a run time of some 60 min.

[31] Figure 7 presents the characteristic ripple height and length that are calculated from the ripple spectra using equations (1) and (2). As with Figure 4 the ripple steepness is calculated as a simple ratio of the height over the length.

[32] Figure 7 shows the same trends as did Figures 5 and 6. The changes in ripple height for both situations is smooth from an original value to their new equilibrium value. The change in ripple length for the decreasing ripples is much more sudden than the corresponding lengthening of the increasing rippled bed. An interesting point in Figure 7 is the change in ripple steepness during the transition period. The ripple steepness is generally constant when the rippled bed is in an equilibrium state. However, as the

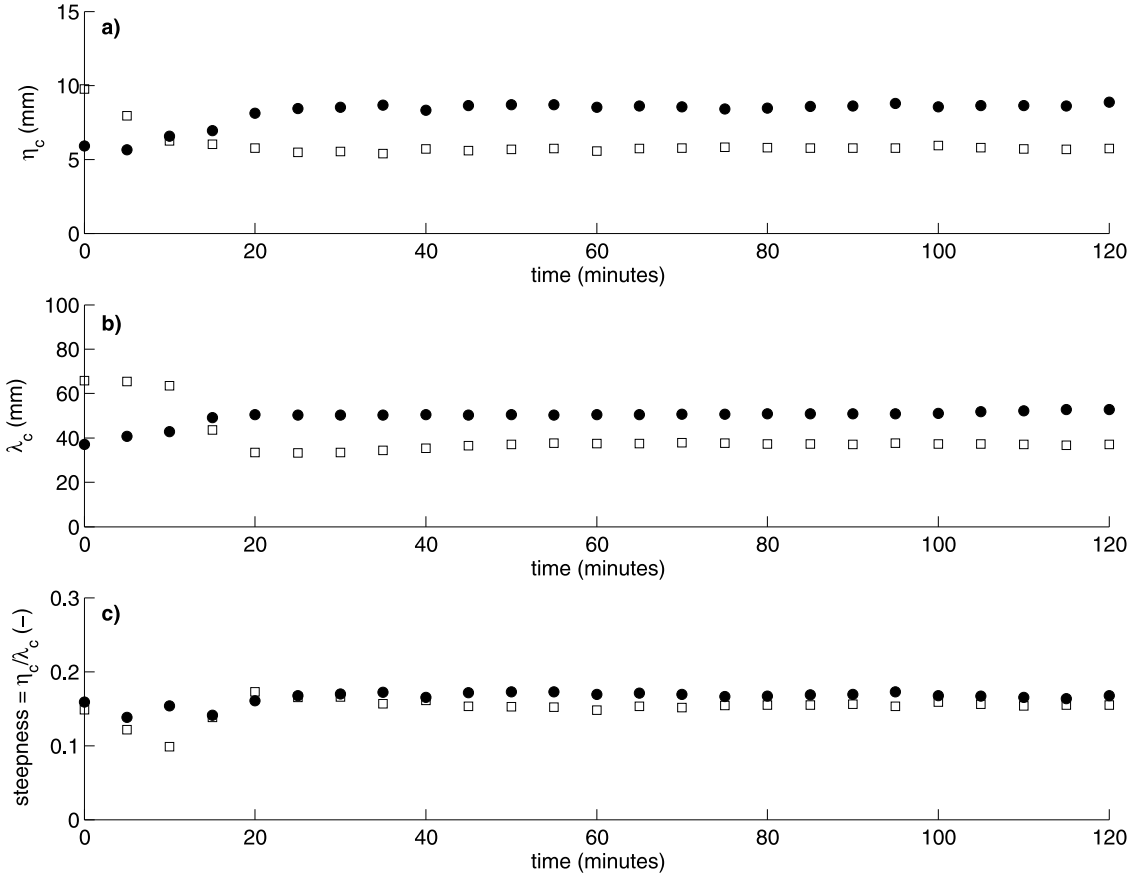

Figure 7. Changes in ripple parameters due to surface waves that are out of equilibrium with the rippled bed. (a) Ripple height. (b) Ripple length.(c) Ripple steepness. The solid circles represent an increase in rippled parameters, while the open squares represent a decrease in ripple parameters.

ripples are transitioning from one equilibrium state to another, there is a corresponding drop in the ripple steepness. This has implications for the modeling of bottom roughness as the roughness height due to ripple forms is generally assumed to be directly proportional to the ripple steepness [*Grant and Madsen*, 1982; *Swart*, 1974; *Raudkivi*, 1988; *Nielsen*, 1992]. Since under real field waves rippled beds may never attain equilibrium [*Traykovski et al.*, 1999], current movable bed models may be overestimating the value of the bottom roughness height.

6. Ripple Bed Evolution Model

[33] The development of a ripple evolution submodel within a general movable bottom roughness model requires not only that the growth of rippled beds from a no-ripple condition be parameterized, as has been done previously [*Nikora and Hicks*, 1997; *Baas*, 1999], but that a more generalized approach be taken that will incorporate the transient nature of ripples between any two equilibrium states. This section develops a method in which the rate of change of the equilibrium spectrum given any two starting energy conditions can be estimated from the flow and sediment parameters.

[34] Studies have been undertaken on the growth of current-formed rippled beds from flat bed conditions that have developed a functional dependence of this growth with time [*Nikora and Hicks*, 1997; *Baas*, 1999]. These functions have been based on the growth of ripples and as such do not take into account the situation presented in Figures 5a in which the overall energy of the rippled bed is reduced due to flow conditions. The formation mechanism of the two species of sediment ripples (current formed and wave formed) are very different, so one would expect that the behavior of these two species under changing flow conditions would also be different.

[35] The ripple transition is driven by the ratio of the fluid energy that acts to move the sediment grains over the ability of the sediment grains to resist movement [*Wiberg and Smith*, 1985]. Previous studies that have developed expressions for equilibrium ripples have used nondimensional ratios loosely based on this observation: mobility number [*Nielsen*, 1981]; period parameter [*Mogridge et al.*, 1994]; and the ratio of the orbital excursion diameter over the sediment grain diameter [*Wiberg and Harris*, 1994]. There is a finite limit to the final potential energy level a rippled bed can achieve due to there being a finite energy level of the ratio discussed above. On the basis of the observations of rippled beds undertaken within this study, rippled beds display two stages of development as they are in the process of transitioning to a new equilibrium state. The first stage is characterized by the transition rate being proportional to the size of ripples present, while during the second stage the opposite is true, with the transition rate being inversely

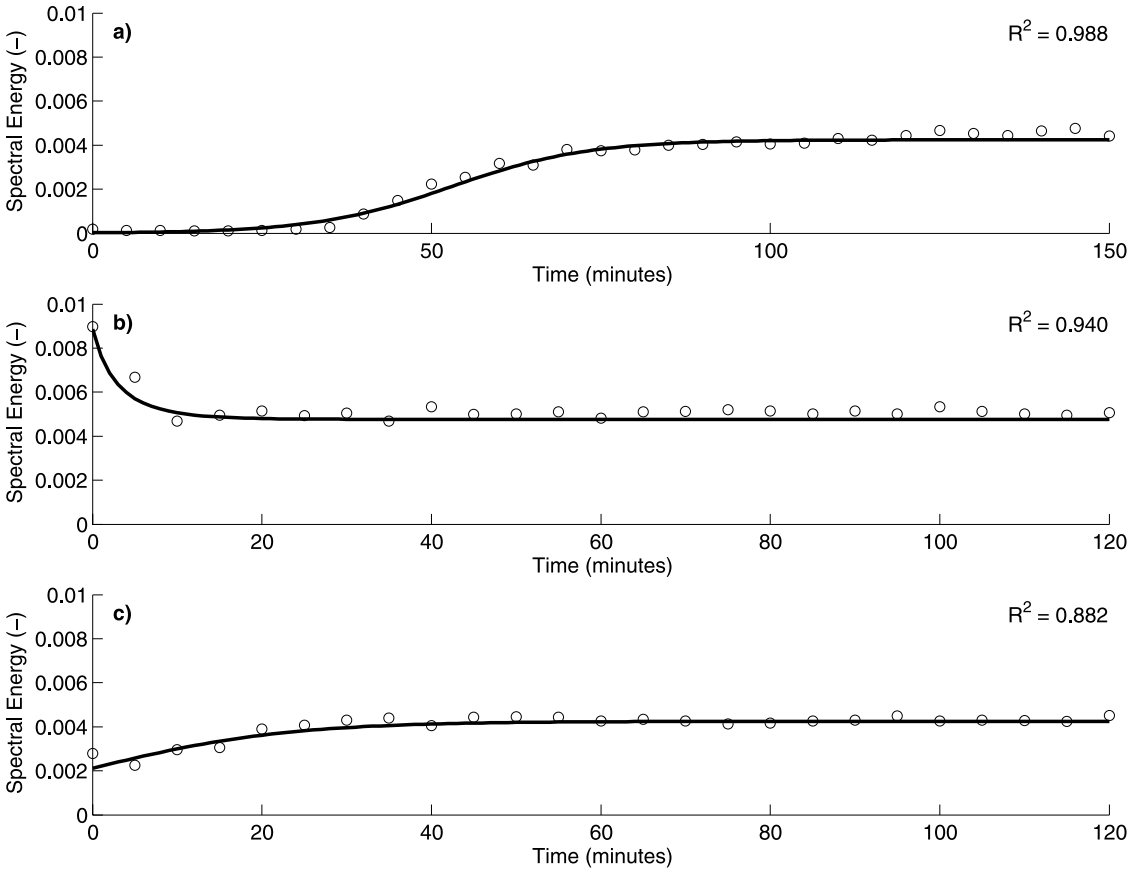

Figure 8. Growth of nondimensional spectral energy with time. (a) Data from Figure 3b. (b) Data from Figure 6b. (c) Data from Figure 6d. The line shows equation (7) fitted to the data set, while the R^2 value is the correlation coefficient of the fit.

proportional to the size of ripples on the bed. This type of growth has been widely described in other areas of science and is know as the Logistic or Verhulst (1804–1849) Growth Law. The Logistic nonlinear differential equation has the form

$$\frac{dE}{dt} = \alpha E(E_f - E), \tag{5}$$

where E is the nondimensional spectral energy level of the bed, t is the time (minutes), α is the evolution rate (1/minutes) and E_f is the new equilibrium nondimensional spectral energy level of the bed. The nondimensional energy of the bed is defined as

$$E = \int_{f_{s1}}^{f_{s2}} S'(f_s')\, df_s'. \tag{6}$$

[36] From equation (5) the rate at which rippled beds evolve can be thought of as a balance between the processes that act to build up the bed and the processes that act to flatten the bed. As the rippled bed is increasing in energy, the factors that influence the growth of the rippled bed dominate over the processes that will cause the bed to flatten until equilibrium is reached and the two factors once again balance. Conversely, as the rippled bed is decreasing in energy, the processes that act to flatten the bed dominate over the growth processes until a new state of equilibrium is reached. The general solution to equation (5) is

$$E = \frac{E_f E_0}{E_0 + (E_f - E_0)\exp(-\alpha E_f t)}, \tag{7}$$

where E_0 is the starting nondimensional spectral energy of the bed. Equation (7) has three fitting parameters: the starting and equilibrium spectral energy levels of the bed and the evolution rate. Figure 8 shows equation (7) fitted to the three example beds discussed within earlier sections and presented in Figures 2 and 5. The three subplots in Figure 8 show equation (7) applied in three different situations using different values of E_f, E_o, and α. These beds represent a bed evolving from a no-ripple condition to an equilibrium bed, a bed evolving from a higher equilibrium state to a lower one, and a bed evolving from a lower equilibrium state up to a higher one.

[37] As can be seen in Figure 8, equation (7) fits the experimental data in the three situations very well with correlation coefficients greater than 0.8 for all cases.

[38] From equation (7) an estimate of the time a rippled bed takes to reach equilibrium can be derived. On the basis of a value suggested by *Baas* [1999], equilibrium was determined to have been reached when the energy level of the bed had reached 99% of its equilibrium value. Setting

Table 3. Summary of Values Obtained From Fitting Equation (7) to the Data Sets

Experimental Test ID	Fitting Parameters			Regression	Equilibrium Time,
	E_0	E_f	α, 1/mm	R^2	min
G01	0.0004	0.0054	6.966	0.980	191.8
G02	0.0001	0.0032	90.116	0.923	30.3
G03	0.0005	0.0040	23.320	0.959	70.0
G04	0.0002	0.0042	36.977	0.989	50.4
G05	0.0000	0.0044	22.993	0.988	98.8
G06	0.0007	0.0043	34.848	0.936	41.5
G07	0.0001	0.0047	22.505	0.976	81.1
G08	0.0001	0.0045	45.676	0.985	42.3
G09	0.0001	0.0046	18.147	0.986	97.2
G10	0.0001	0.0037	47.325	0.977	46.8
G11	0.0002	0.0038	21.363	0.984	96.8
G12	0.0003	0.0051	15.764	0.990	90.7
G13	0.0037	0.0050	5.124	0.832	137.2
G14	0.0004	0.0045	36.185	0.962	42.0
G15	0.0003	0.0052	12.349	0.984	116.5
G16	0.0004	0.0044	9.279	0.953	166.8
G17	0.0003	0.0041	18.697	0.982	93.1
G18	0.0000	0.0059	9.698	0.981	230.7
G19	0.0003	0.0034	34.683	0.954	58.7
G20	0.0007	0.5856	0.007	0.813	2677.5
T01	0.0072	0.0042	56.478	0.588	15.7
T02	0.0100	0.0052	1.932	0.981	384.3
T03	0.0077	0.0042	49.432	0.940	18.6
T04	0.0068	0.0036	85.079	0.728	12.4
T05	0.0032	0.0051	7.282	0.911	108.9
T06	0.0025	0.0050	4.582	0.893	199.7
T07	0.0022	0.0043	20.233	0.882	52.6
T08	0.0025	0.0043	21.410	0.906	45.8
T09	0.0007	0.0047	21.235	0.989	64.1

the left-hand side of equation (7) to equal $0.99E_f$ and solving the equation for time gives

$$t_e = \frac{-1}{\alpha E_f} \ln\left[\frac{0.01E_0}{0.99(E_f - E_0)}\right], \tag{8}$$

where t_e is the equilibrium time in minutes. The time a rippled bed takes to reach equilibrium will not only be a function of the evolution rate, but also of the initial and final conditions of the bed.

[39] Table 3 shows the results of fitting equation (7) to all the data sets presented in Tables 1 and 2, including how the fit correlated with the data set and the time to reach equilibrium. Note that flow and sediment parameters for the tests starting with "G" (growth) are listed in Table 1, while those starting with "T" (transition) are listed in Table 2. As can be seen in Table 3, all 29 tests fit equation (7) well, with R^2 values ranging from 0.990 down to 0.588. The growth tests fitted equation (7) slightly better than did the transition test that overall had lower R^2 values. The time for the bed to reach equilibrium calculated via equation (8) is also presented in Table 3. As can be seen, these times range anywhere from 12 min (T04) to 2680 min (G20). Test G20 was undertaken with deeper water and very low surface wave conditions and as such did not form a stable ripple bed during the test time; however, it is included here to show that the method will work as long as there is a change in ripple conditions between the start and finish of the experimental test.

[40] The main purpose of this paper is to enable the temporal changes that a rippled beds undergoes to be modeled; hence, it is important to be able to estimate the evolution rate from flow conditions and sediment properties. From the values listed in Tables 1, 2, and 3, a relationship between four of the more widely used non-dimensional numbers and the evolution rate can be derived. It was determined that of the four nondimensional numbers shown in Tables 1 and 2, the skin friction Shields parameter provided the best correlation with the evolution rate. Figure 9 shows the relationship developed between the evolution rate and the skin friction Shields parameter.

[41] There is a significant correlation ($p < 0.01$) in Figure 9 between the Shields parameter and the evolution rate; however, the correlation is low, with large experimental scatter shown in the data set. The evolution rate can be calculated as a function of the skin friction Shields parameter using the following relationship:

$$\alpha = 5.11 \times 10^6 \theta^{5.79}. \tag{9}$$

This function was determined by fitting a straight line to the data set in log-log space. It shows that increasing the Shields parameter by a small amount will cause the rate of ripple evolution to increase by a substantially higher rate.

[42] There is no appreciable difference between the values of the evolution rate determined from the growth tests and the transition tests in Figure 9. This would indicate that ripple growth and transition can be considered to be the same process, which is adequately modeled by the nonlinear differential logistic equation (equation (5)).

7. Discussion

[43] As shown in section 4, ripple forms do not develop uniformly over a sediment surface under the action of irregular surface waves, but initially appear as patches of ripples that merge together over time. The location where ripples will start to develop is impossible to estimate due to the heterogeneous nature of sediment beds and the random fluctuations of flow properties under irregular surface waves. How quickly these patches of ripples merge and develop into a fully developed rippled bed will be dependent on the flow and sediment properties. Hence current methods to parameterize rippled beds based on a single value for the ripple height and length will be prone to errors in situations where the rippled bed is actively growing from a no-ripple condition. A far better way to describe transient rippled beds is to parameterize the whole bed in terms of its spectral density function. Changes in ripple parameters at one location of the bed do not determine the parameters for the whole bed, but are averaged out across a given area of the bed. This allows the spatial variability in ripple properties to be factored into the transient analysis of rippled beds.

[44] The ripple evolution model described in section 6 shows that the evolution of a rippled bed between two equilibrium states can be described mathematically in exactly the same way as a rippled bed growing from a no-ripple condition. There is no difference in the experimentally determined values of the evolution rate calculated from the ripple growth tests and the ripple transition tests (refer to Figure 9). If the initial and final energy levels of a given bed can be calculated, then the rate at which these

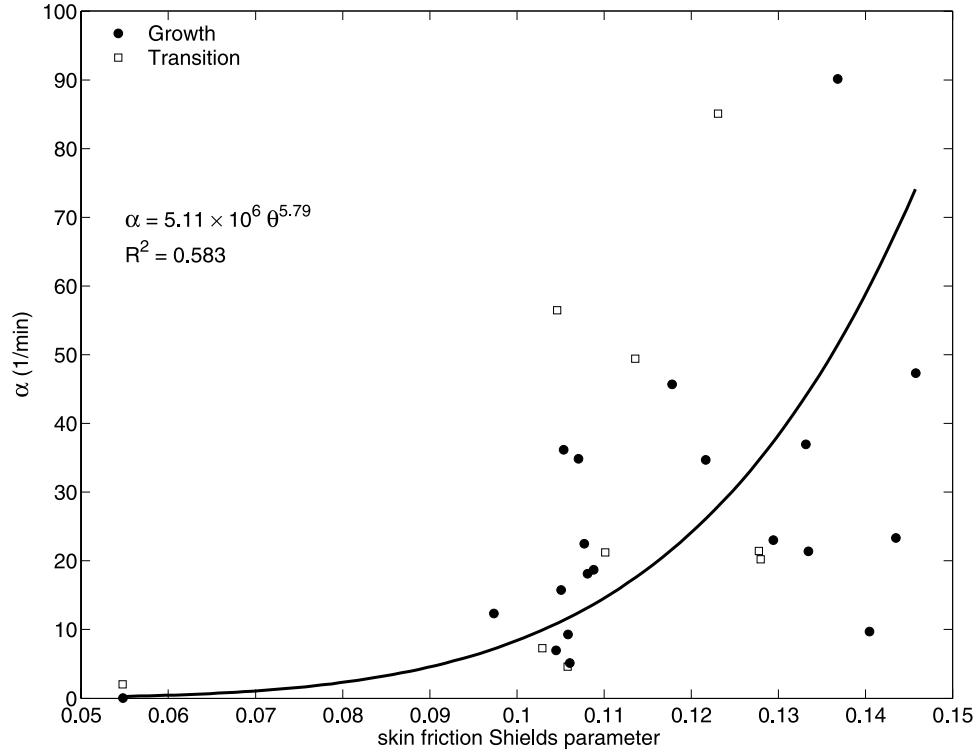

Figure 9. Relationship between the evolution rate and the skin friction Shields parameter. The solid circles represent growth tests, while the open squares represent transition tests.

beds will change can be determined from the flow and sediment properties via equation (9).

[45] Ripple transition experiments undertaken within this study could only focus on very small-scale long crested ripples that were generated under a narrow range of surface wave conditions. This meant that rippled beds only transitioned between two states that were in the same order of scale and that the ripple profile was only changing along the axis of the wave propagation. This was not seen as a constraint to the future application of the ripple evolution model to any given rippled bed that is in the process of actively changing between two equilibrium states. Recently, *Lyons et al.* [2002] described a method to characterize an area of the seafloor in terms of its two-dimensional spectrum. As is the case with estimations of the significant wave height from the water surface spectrum, the area under the nondimensional ripple spectrum could be calculated just as easily from a two-dimensional ripple spectrum instead of the one-dimensional spectrum as was done in this study. However, to adequately nondimensionalize a ripple spectrum calculated from an area of the sediment bed containing so-called three-dimensional ripple forms would require the understanding of the formation mechanisms for these types of beds to be substantially improved. *Traykovski et al.* [1999] observed rippled beds, containing two very different scales of ripples, actively changing between energy states due to a change in the surface wave conditions at the LEO-15 site. From a spectral point of view, this would give a double peaked spectral plot. Side-scan sonar plots presented by *Traykovski et al.* [1999] showed smaller ripples growing on top of large older remnant ripples. As the newer ripples developed, the older ripples disappeared, which would suggest that there was a redistribution of spectral energy from low to high spatial frequencies in the spectral density function of this bed. As the spectral energy shifted, the total energy of the bed would certainly have changed, and it is this change in spectral energy that the ripple evolution model seeks to describe. Hence the application of the ripple evolution model is not constrained by the limited scale of measurements undertaken during this study.

[46] Prior to the evolution model, described in section 6, being applied in an operational wave forecasting model, a number of practical issues need to be resolved or researched further. The most obvious issue is the estimation of the initial and final energy states of the sediment bed. The estimation of the nondimensional ripple spectrum from flow conditions and sediment parameters is an area of active research by the authors. The application would proceed in much the same way as current movable bottom roughness models proceed. At the end of each time step, in a transient wave model, a new bed configuration would be estimated based on the flow conditions and sediment bed properties calculated at the previous time step. However, there would not be the underlying assumption that the ripple field is in constant equilibrium with the wave field, as is the case with current movable bed roughness models [*Tolman*, 1995]. On the basis of flow conditions and time step length, the ripple parameters and hence the bottom roughness height would be scaled back from equilibrium values. This would allow the rippled bed to be modeled more realistically as the simulation proceeds. Another issue in applying the ripple evolution model is the determination of a starting value for the nondimensional spectral energy in the simulation. If the value of the initial state of the bed is set to zero, then

equation (7) predicts zero energy for all subsequent values of t. Hence an initial value of E_o is required by the approach. Within the current paper the value of the nondimensional spectral energy for the sediment beds in a no-rippled state were on the order of 10^{-4}, which was generally an order of magnitude lower than the final states; hence, a similar small value could be used to start a modeling simulations from which the simulation would ramp up.

[47] Issues such as bioturbated beds [*Wheatcroft*, 1994] could be incorporated into the evolution model by estimating the background spectral energy of such beds. If wave conditions were so low as to not cause the bed to evolve, then the rate at which benthic organisms rework the bed could be incorporated into the analysis. *Amos et al.* [1988] suggests that benthic organisms will degrade rippled beds to a ''flat'' bed condition within 4 to 6 hours.

[48] The next step forward would be to develop the evolution model into a full two-dimensional model that would incorporate a dependence on the peak surface wave direction. However, issues such as the isotropic nature of bioturbated or ''flat'' sediment beds would have to be factored into the analysis. As wave-formed ripples develop, the sediment bed changes from isotropic to anisotropic in nature [*Briggs et al.*, 2002].

8. Summary and Conclusion

[49] A new method has been presented that uses the spectral density function of small-scaled wave-formed rippled sediment beds to model the changes a rippled bed undergoes as it actively evolves between two given equilibrium states due to a change in surface wave conditions. The method developed is based on a series of experimental tests undertaken within a flume setting. The rippled beds were forced to change by using random irregular waves conforming to a standard JONSWAP spectrum that were out of equilibrium with the original bed condition. Two equilibrium states were considered, the first being a flat bed condition that was in equilibrium with a no-wave surface condition, while the other was a fully developed ripple bed that is in equilibrium with the surface waves that originally formed that bed. The evolving ripple bed was scanned every 5 min using a laser scanning system, enabling a time series of the rippled bed to be developed.

[50] The ripple evolution model was developed from the well-known Logistic Growth Law. Using this growth model, changes in the spectral energy level of the bed can be thought of as a balance between the processes that act to build up the bed and the processes that act to flatten a bed. Fitting the general solution of the logistic nonlinear differential equation to the experimental data enabled the evolution rate of the bed to be determined for each experimental test.

[51] It was concluded that there was no difference between the evolution rate determined from the ripple growth tests and the ripple transition tests. This indicated that the two types of growth are special cases of the same evolution processes. A functional dependence was established between the ripple evolution rate and the Shields parameter. This allows the evolution rate to be estimated from flow and sediment properties. The estimation of the rate at which rippled sediment beds evolve under a variable sea state has the potential to lead to significant improvements in the way ripple transition and hence bottom roughness is approximated in coastal wave models.

Notation

A	bottom orbital semi-excursion amplitude, m.
D_{50}	50 percentile sediment diameter, m.
d_{op}	peak bottom orbital excursion diameter, m.
E	spectral energy level.
E_0	initial spectral energy level.
E_f	final spectral energy level.
f_s	ripple spatial frequency, 1/m.
f_s'	non-dimensional ripple spatial frequency.
H_s	significant wave height, m.
p	statistical correlation test.
Re	flow Reynolds number.
Re_d	sediment Reynolds number.
S_r	ripple variance spectrum, m^3.
S'	non-dimensional ripple spectrum.
t	time, min.
t_e	equilibrium time, min.
U_p	peak bottom orbital velocity, m/s.
U_{rms}	root mean squared bottom orbital velocity, m/s.
α	ripple evolution rate, 1/min.
γ	JONSWAP peak factor.
η_c	characteristic ripple height, m.
θ	skin friction Shields parameter.
λ_c	characteristic ripple length, m.
σ_p	peak surface wave frequency, Hz.
ψ	mobility number.

[52] **Acknowledgments.** The authors would like to acknowledge the role of the Australian Research Council in providing funding for this project under the SPIRT scheme and the Coast Protection Board of South Australia as the industry partner (grant C00107520). We would like to thank: Alex Babanin of the University of Adelaide, Australia, for some useful discussions on the application of spectral analysis methods; Mark Donelan of the University of Miami, USA, for providing the original FFT bandpassing code; and Tom O'Donoghue of the University of Aberdeen, UK, for his advice regarding the laser displacement sensor used in the ASILS measurement system. We are grateful to Peter Traykovski and an anonymous reviewer for their constructive comments which contributed to the paper.

References

Amos, C., A. Bowen, D. Huntley, and C. Lewis (1988), Ripple generation under the combined influences of waves and currents on the Canadian continental shelf, *Cont. Shelf Res.*, *8*(10), 1129–1153.

Baas, J. (1999), An empirical model for the development and equilibrum morphology of current ripples in fine sand, *Sedimentology*, *46*, 123–138.

Bagnold, R. (1946), Motion of waves in shallow water, *Proc. R. Soc. London, Ser. A*, *187*, 1–15.

Bell, P., and P. Thorne (1997), Measurements of sea bed ripple evolution in an estuarine environment using a high resolution acoustic sand ripple profiling system, paper presented at Oceans '97, Inst. for Elect. and Elect. Eng., Halifax.

Briggs, K., D. Tang, and K. Williams (2002), Characterization of interface roughness of rippled sand off Fort Walton Beach, Florida, *IEEE J. Oceanic Eng.*, *27*(3), 505–514.

Coleman, S., and B. Melville (1996), Initiation of bed forms on a flat sand bed, *J. Hydraul. Eng.*, *122*(6), 301–310.

Dade, W., A. Hogg, and B. Boudreau (2001), Physics of flow above the sediment-water interface, in *The Benthic Boundary Layer*, edited by B. Boudreau and B. Jorgensen, pp. 4–43, Oxford Univ. Press, New York.

Davis, J., D. Walker, M. Townsend, and I. Young (2003), Spectral description of small scale wave formed rippled sediment beds, in *Proceedings of the International Conference on Coastal Sediments 2003* [CD-ROM], World Sci., River Edge, N. J.

Doucette, J. (2002), Bedform migration and sediment dynamics in the nearshore of a low-energy sand beach in southwest Australia, *J. Coastal Res.*, *18*(3), 576–591.

Drake, D., and D. Cacchione (1989), Estimates of the suspended sediment reference concentration (ca) and resuspension coefficient (go) from near-bottom observations on the California Shelf, *Cont. Shelf Res.*, *9*(1), 51–64.

Faraci, C., and E. Foti (2002), Geometry, migration and evolution of small-scale bedforms generated by regular and irregular waves, *Coastal Eng.*, *47*, 35–52.

Goda, Y. (2000), *Random Seas and Design of Maritime Structures*, 2nd ed., *Adv. Ser. Ocean Eng.*, vol. 15, World Sci., River Edge, N. J.

Graber, H., and O. Madsen (1988), A finite-depth wind-wave model: 1. Model description, *J. Phys. Oceanogr.*, *18*(11), 1465–1483.

Grant, W., and O. Madsen (1982), Movable bed roughness in unsteady oscillatory flow, *J. Geophys. Res.*, *87*(C1), 469–481.

Huettel, M., and I. Webster (2001), Porewater flow in permeable sediments, in *The Benthic Boundary Layer*, edited by B. Boudreau and B. Jorgensen, pp. 144–179, Oxford Univ. Press, New York.

Jain, S., and J. Kennedy (1974), The spectral evolution of sedimentary bed forms, *J. Fluid Mech.*, *63*(2), 301–314.

Jorgensen, B., and B. Boudreau (2001), Diagenesis and sediment-water exchange, in *The Benthic Boundary Layer*, edited by B. Boudreau and B. Jorgensen, pp. 211–244, Oxford Univ. Press, New York.

Lyons, A., W. Fox, T. Hasiotis, and E. Pouliquen (2002), Characterization of the two-dimensional roughness of wave-rippled sea floors using digital photgrammetry, *IEEE J. Oceanic Eng.*, *27*(3), 515–524.

Marsh, S., C. Vincent, and P. Osborne (1999), Bedforms in a laboratory wave flume: An evaluation of predictive models for bedform wavelengths, *J. Coastal Res.*, *15*(3), 624–634.

Mogridge, G., M. Davies, and D. Willis (1994), Geometry prediction for wave-generated bedforms, *Coastal Eng.*, *22*, 255–286.

Moore, K., and J. Jaffe (2002), Time-evolution of high-resolution topographic measurements of the sea floor using a 3-D laser line scan mapping system, *IEEE J. Oceanic Eng.*, *27*(3), 525–545.

Nielsen, P. (1981), Dynamics and geometry of wave-generated ripples, *J. Geophys. Res.*, *86*(C7), 6467–6472.

Nielsen, P. (1992), *Coastal Bottom Boundary Layers and Sediment Transport*, *Adv. Ser. Ocean Eng.*, vol. 4, World Sci., River Edge, N. J.

Nikora, V., and D. Hicks (1997), Scaling relationships for sand wave development in unidirectional flow, *J. Hydraul. Eng.*, *123*(12), 1152–1156.

O'Donoghue, T., and G. Clubb (2001), Sand ripples generated by regular oscillatory flow, *Coastal Eng.*, *44*, 101–115.

Raudkivi, A. (1988), The roughness height under waves, *J. Hydraul. Res.*, *26*(5), 569–584.

Soulsby, R. (1987), Calculating bottom orbital velocity beneath waves, *Coastal Eng.*, *11*, 371–380.

Swart, D. (1974), Offshore sediment transport and equilibrium beach profiles, *Tech. Rep. Pub. 131*, Delft Hydraul. Lab., Delft, Netherlands.

Tolman, H. (1994), Wind waves and moveable bed bottom friction, *J. Phys. Oceanogr.*, *24*(5), 994–1009.

Tolman, H. (1995), Subgrid modeling of moveable-bed bottom friction in wind wave models, *Coastal Eng.*, *26*, 57–75.

Traykovski, P., E. Hay, A. J. Irish, and J. Lynch (1999), Geometry, migration, and evolution of wave orbital ripples at Leo-15, *J. Geophys. Res.*, *104*(C1), 1505–1524.

Wheatcroft, R. (1994), Temproal variation in bed configuration and one-dimensional bottom roughness at the mid-shelf stress site, *Cont. Shelf Res.*, *14*(10/11), 1167–1190.

Wiberg, P., and C. Harris (1994), Ripple geometry in wave-dominated environments, *J. Geophys. Res.*, *99*(C1), 775–789.

Wiberg, P., and J. Smith (1985), A theoretical model for saltating grains in water, *J. Geophys. Res.*, *90*(C4), 775–789.

Young, I. (1995), The determination of confidence limits associated with estimates of the spectral peak frequency, *Ocean Eng.*, *22*(7), 669–689.

J. P. Davis and D. J. Walker, School of Civil and Environmental Engineering, University of Adelaide, Adelaide, South Australia 5005, Australia. (jdavis@civeng.adelaide.edu.au; dwalker@civeng.adelaide.edu.au)

M. Townsend, Department for Environment and Heritage, GPO Box 1047, Adelaide, South Australia 5001, Australia. (townsend.murray@saugov.sa.gov.au)

I. R. Young, Swinburne University of Technology, PO Box 218, Hawthorn, Melbourne, Victoria 3122, Australia. (iyoung@swin.edu.au)